LETTER

doi:10.1038/nature11902

Observation of quantum state collapse and revival due to the single-photon Kerr effect

Gerhard Kirchmair[1], Brian Vlastakis[1], Zaki Leghtas[2], Simon E. Nigg[1], Hanhee Paik[1], Eran Ginossar[3], Mazyar Mirrahimi[1,2], Luigi Frunzio[1], S. M. Girvin[1] & R. J. Schoelkopf[1]

To create and manipulate non-classical states of light for quantum information protocols, a strong, nonlinear interaction at the single-photon level is required. One approach to the generation of suitable interactions is to couple photons to atoms, as in the strong coupling regime of cavity quantum electrodynamic systems[1,2]. In these systems, however, the quantum state of the light is only indirectly controlled by manipulating the atoms[3]. A direct photon–photon interaction occurs in so-called Kerr media, which typically induce only weak nonlinearity at the cost of significant loss. So far, it has not been possible to reach the single-photon Kerr regime, in which the interaction strength between individual photons exceeds the loss rate. Here, using a three-dimensional circuit quantum electrodynamic architecture[4], we engineer an artificial Kerr medium that enters this regime and allows the observation of new quantum effects. We realize a gedanken experiment[5] in which the collapse and revival of a coherent state can be observed. This time evolution is a consequence of the quantization of the light field in the cavity and the nonlinear interaction between individual photons. During the evolution, non-classical superpositions of coherent states (that is, multi-component 'Schrödinger cat' states) are formed. We visualize this evolution by measuring the Husimi *Q* function and confirm the non-classical properties of these transient states by cavity state tomography. The ability to create and manipulate superpositions of coherent states in such a high-quality-factor photon mode opens perspectives for combining the physics of continuous variables[6] with superconducting circuits. The single-photon Kerr effect could be used in quantum non-demolition measurement of photons[7], single-photon generation[8], autonomous quantum feedback schemes[9] and quantum logic operations[10].

A material whose refractive index depends on the intensity of the light field is called a Kerr medium. A light beam travelling through such a material acquires a phase shift $\phi_{\mathrm{Kerr}} = K\tau I$ (ref. 11), where K is the Kerr constant, τ is the interaction time of the light field with the material, and I is the intensity of the beam. The Kerr effect is a widely used phenomenon in nonlinear quantum optics, and has been successfully used to generate quadrature and amplitude squeezed states[12], parametrically convert frequencies[13], and create ultra-fast pulses[14]. In the field of quantum optics with microwave circuits, the direct analogue of the Kerr effect is naturally created by the nonlinear inductance of a Josephson junction (specifically the $\phi^4 \propto (b + b^\dagger)^4$ term in the Taylor expansion of $\cos\phi$ in the Josephson energy relation, where ϕ is the superconducting phase difference across the junction, and b and $b^\dagger$ are the corresponding ladder operators)[15,16]. This effect has been used to create Josephson parametric amplifiers[17] and to generate squeezing of microwave fields[18]. However, in both the microwave and optical domains, most experiments use the Kerr nonlinearity in a semi-classical regime, where the quantization of the light field does not play a crucial role. The Kerr effect for a quantized mode of light with frequency ω_c can be described by the normal ordered Hamiltonian, $H_{\mathrm{Kerr}} = \hbar\omega_c a^\dagger a - \hbar\frac{K}{2} a^\dagger a^\dagger aa$, with K the Kerr frequency shift per photon[2,16] and $a/a^\dagger$ the ladder operators. The average phase shift per photon is again given by $\phi_{\mathrm{Kerr}} = K/\kappa$, with κ the decay rate of the photon mode. Typical Kerr effects are so small that they are not visible on the single-photon level because $\kappa > K$. Applications which require K much bigger than κ include the realization of quantum logic operations[10], schemes for continuous variable quantum information protocols[6] and quantum non-demolition measurements of propagating photons[7].

The Kerr nonlinearity of a Josephson junction is also routinely used to create superconducting qubits. In this case, a circuit is engineered with such a strong anharmonicity that it can be considered as a two-level system. By combining a qubit with linear resonators, one realizes the analogue of strong coupling cavity quantum electrodynamics (QED), known as circuit QED[1]. This can be used to protect the qubit from spontaneous emission, manipulate and read out its quantum state and couple it to other qubits. One consequence of coupling any resonator to a qubit is that the resonator always acquires a finite anharmonicity K, becoming a Kerr medium itself[15]. Here we have designed K large enough ($K/\kappa > 30$) to be well within the single-photon Kerr regime. At the same time, the nonlinearity is small enough that short pulses ($t_{\mathrm{pulse}} \approx 10$ ns $\ll 1/K$) applied to the resonator create a coherent state, allowing us to conveniently access the large Hilbert space of the oscillator. Only a few experiments have previously come close to the limit where $K/\kappa \approx 1$ while still maintaining the ability to create coherent states[19–21]. So far no experiment has been able to satisfy both conditions at the same time so as to observe the collapse and revival of a coherent state due to the Kerr effect.

As a first demonstration within this single-photon Kerr regime, we realize a proposal[5] for creating photonic Schrödinger cat states. Specifically, we generate coherent states with a mean photon number of up to four photons and measure the Husimi Q function of the resonator state using a new experimental measurement protocol. We then show the high quality of the Kerr resonator by measuring the time evolution of the collapse and revival of a coherent state. During the evolution, highly non-classical superpositions of coherent states, that is, multi-component Schrödinger cat states, are formed, which show the coherent nature of the effect. This revival, in contrast to the Jaynes–Cummings revival of Rabi oscillations of a qubit induced by a coherent state[2,22], is the revival of a coherent state in a resonator. An analogous effect was indirectly observed in early experiments with a condensate of bosonic atoms in an optical lattice[23]. Additionally, we confirm the non-classical properties of the transient states by performing cavity state tomography.

We experimentally realize a highly coherent Kerr medium by coupling a superconducting 'vertical' transmon qubit to two three-dimensional waveguide cavities, as shown in Fig. 1a. This design is based on a recently developed three-dimensional circuit QED architecture[4]. The two halves of the cavities are machined out of a block of superconducting aluminium (alloy 6061 T6). Both cavities have a total quality

[1]Departments of Physics and Applied Physics, Yale University, New Haven, Connecticut 06511, USA. [2]INRIA Paris-Rocquencourt, Domaine de Voluceau, BP 105, 78153 Le Chesnay Cedex, France. [3]Department of Physics and Advanced Technology Institute, University of Surrey, Guildford, Surrey GU2 7XH, UK.

factor of about one million, limited by internal losses, corresponding to a single-photon decay rate $\kappa/2\pi = 10$ kHz. The vertical transmon consists of a single Josephson junction embedded in a transmission line structure, which couples the junction to both cavities. The observed transition frequency of the qubit is $\omega_q/2\pi = 7.8503$ GHz and its anharmonicity is $K_q/2\pi = (\omega_{ge} - \omega_{ef})/2\pi = 73.4$ MHz using the standard convention for labelling from lowest to highest energy level in the qubit as $(g,e,f,h,\ldots)$ (see Supplementary Information). The energy relaxation time of the qubit is $T_1 = 10$ µs with a Ramsey time $T_2^* = 8$ µs. The qubit is used to interrogate the state of the storage cavity, which acts as a Kerr medium. The other cavity is used to read out the state of the qubit after the interrogation, similarly to ref. 24.

The analysis of the distributed stripline elements and the cavity electrodynamics can be performed using finite-element calculations for the actual geometry. Combined with 'black-box' circuit quantization[15], one can derive dressed frequencies, couplings and anharmonicities with good relative accuracy (see Supplementary Information). For the purposes of the experiments discussed here, the coupling of the qubit to the storage resonator, in the strong dispersive limit of circuit QED, is well described by the Hamiltonian

$$\frac{H}{\hbar} = \frac{\omega_q}{2}\sigma_z - \frac{\chi}{2}a^\dagger a\sigma_z + \left(\omega_c - \frac{\chi}{2}\right)a^\dagger a - \frac{K}{2}a^\dagger a^\dagger a a \qquad (1)$$

taking into account only the lowest two energy levels of the qubit. The operators $a^\dagger/a$ are the usual raising/lowering operators for the harmonic oscillator and σ_z is the Pauli operator. In this description, we completely omit the measurement cavity because it is only used for reading out the state of the qubit and otherwise stays in its ground state. The energy level diagram described by the Hamiltonian given in equation (1) can be seen in Fig. 1b. The second term on the right-hand side of equation (1) is the state-dependent shift per photon $\chi/2\pi = 9.4$ MHz of the qubit transition frequency. The last two terms on the right-hand side of equation (1) describe the cavity as an anharmonic oscillator with a dressed resonance frequency ω_c and a nonlinearity $K/2\pi = 325$ kHz which is given by $K \approx \chi^2/4K_q$ (ref. 15). All interaction strengths in the above Hamiltonian are at least one order of magnitude bigger than any decoherence rate in the system.

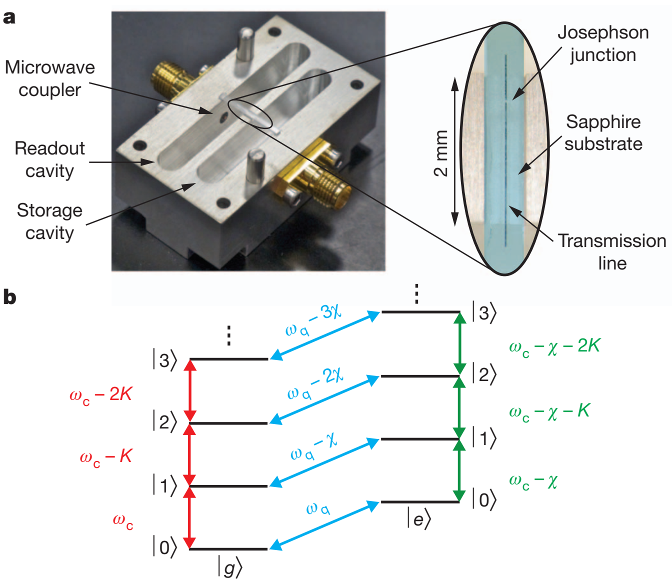

Figure 1 | Device layout and energy level diagram of the two-cavity, one-qubit device. **a**, Photograph of one half of two aluminium (alloy 6061) waveguide cavities coupled to a vertical transmon qubit. Right, a magnified view of the indicated area of the photograph, showing a detail of the qubit, fabricated on a *c*-plane sapphire substrate 1.4 mm wide, 15 mm long and 430 µm thick. The coupling strength of the qubit is determined by the length of the stripline coupling antenna which extends into each cavity. The upper cavity, with a resonant frequency of $\omega_m/2\pi = 8.2564$ GHz, is used for qubit readout, and the lower cavity, with a frequency of $\omega_c/2\pi = 9.2747$ GHz, is used to store and manipulate quantum states. **b**, Combined energy level diagram of the qubit coupled to the storage cavity. The qubit states are denoted as $|g\rangle$ and $|e\rangle$, respectively, while the cavity states are labelled as $|n\rangle$, with n the number of photons in the cavity. Each photon in the cavity reduces the qubit transition frequency by χ. Equivalently, exciting the qubit reduces the cavity transition frequency by χ. The energy levels of the cavity are not evenly spaced owing to the induced Kerr anharmonicity, $K/2\pi = 325$ kHz.

To visualize and understand the evolution of the resonator state, we measure the Husimi Q function Q_0 in a space spanned by the expectation value of the dimensionless field quadratures $\mathrm{Re}(\alpha)$ and $\mathrm{Im}(\alpha)$. Q_0 is defined as the modulus squared of the overlap of the resonator state $|\Psi\rangle$ with a coherent state $|\alpha\rangle$ by $Q_0(\alpha) = \frac{1}{\pi}|\langle\alpha|\Psi\rangle|^2$. Alternatively, we can write Q_0 using the displacement operator $D_\alpha = e^{\alpha a^\dagger - \alpha^* a}$ (note that $D_\alpha^\dagger = D_{-\alpha}$) as $Q_0(\alpha) = \frac{1}{\pi}|\langle 0|D_{-\alpha}|\Psi\rangle|^2$, which describes the actual measurement procedure used in the experiment. The sequence to measure Q_0 can be seen in Fig. 2a. The initial displacement, D_β, creates a coherent state $|\Psi\rangle = |\beta\rangle$ in the cavity, whose Q_0 is given by a Gaussian, $\frac{1}{\pi}e^{-|\alpha-\beta|^2}$. After a variable waiting time t, we measure $Q_0(\alpha)$ by displacing the cavity state by $-\alpha$ and determine the overlap of the resulting wavefunction with the cavity ground state. The population of the cavity ground state can be measured by applying a photon number state selective π pulse, $X_\pi^{n=0}$, to the qubit (see Supplementary Information), similarly to ref. 25. The qubit is excited if and only if the cavity is in the $n = 0$ Fock state, n being the photon number, after the analysis displacement. This scheme allows us to determine $Q_0(\alpha)$ of the resonator up to experimental imperfections (see Supplementary Information for details). Applying π pulses to the qubit conditioned on other photon numbers, X_π^n, allows us to measure the overlap of the displaced state with any Fock state n, which we will call the generalized Q functions $Q_n(\alpha) = \frac{1}{\pi}|\langle n|D_{-\alpha}|\Psi\rangle|^2$. In essence, we can ask the question 'are there n photons in the resonator?', using photon number state selective pulses[24]. To test the analysis protocol, we measured Q_0 and Q_1 of the cavity in the ground state, Fig. 2b–e, by omitting the first displacement pulse of the sequence given in Fig. 2a.

Using this method, we can follow the time evolution of a coherent state in the presence of the Kerr effect. In the experiment, we prepare a coherent state with an average photon number $|\beta|^2 = \bar{n} = 4$ using a microwave pulse[21] to displace the cavity state. We then measure Q_0 for different delays between the preparation and analysis pulses. A comparison of the theoretical evolution of the coherent state and the measured evolution can be seen in Fig. 3. The time evolution of the state is described by considering the action of the Kerr Hamiltonian H_{Kerr} on a coherent state $|\beta\rangle$ in the cavity[5,26]. In the rotating frame of the harmonic oscillator, with the qubit in the ground state, we can write:

$$|\Psi(t)\rangle = e^{i\frac{K}{2}(a^\dagger a)^2 t}|\beta\rangle = e^{-|\beta|^2/2}\sum_n \frac{\beta^n}{\sqrt{n!}}e^{i\frac{K}{2}n^2}|n\rangle \qquad (2)$$

For short times, the nonlinear phase evolution of the Fock states $|n\rangle$ is closely approximated by a rotation of the state with an angle $\phi_{\mathrm{Kerr}} = Kt(|\beta|^2 + 1/2)$ with respect to the frame rotating at ω_c. The onset of this rotation can be seen in Fig. 3a, which is taken at the minimal waiting time of 15 ns between the two displacement pulses. Because of this waiting time, the state rotates under the influence of the Kerr effect from $\beta = 2$ to $\beta e^{i\phi_{\mathrm{Kerr}}} = 2e^{i0.13}$. For longer times we can see how the state rotates further and spreads out on a circle (Fig. 3b, c). This spreading can be simply understood in a semi-classical picture, in which the amplitude components in the coherent state further away from the origin evolve with a higher angular velocity given by the n^2 dependence of the Kerr effect. Complete phase collapse is reached at a time when the phase dispersion across the width of the photon number distribution corresponds to $\sim\pi$, which can be estimated as $T_{\mathrm{col}} = \frac{\pi}{2\sqrt{\bar{n}}K}$ (ref. 2). For our system, the complete phase collapse

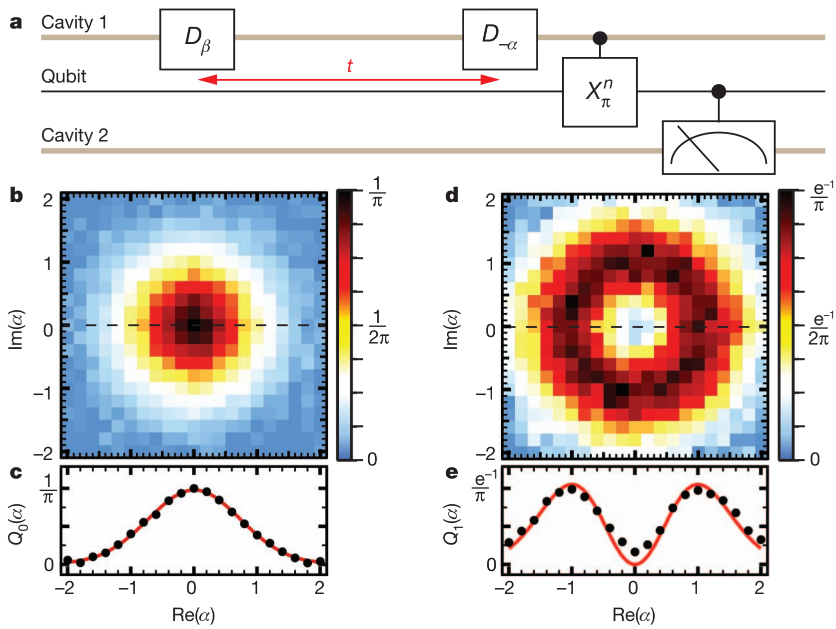

Figure 2 | Technique for measuring the generalized Husimi Q functions. **a**, The experimental pulse sequence consists of a 10-ns displacement pulse D_β, which creates a coherent state in the cavity. After a variable waiting time, t, we analyse the state in the cavity by displacing the cavity by $-\alpha$ followed by a π pulse on the qubit conditioned on having n photons in the cavity. In this way we can measure the generalized Q functions, $Q_n(\alpha)=\frac{1}{\pi}|\langle n|D_{-\alpha}|\Psi\rangle|^2$, which are projections of the displaced wavefunction onto the Fock states $|n\rangle$, where $Q_0(\alpha)$ is the Husimi Q function. **b**, Density plot of Q_0 of the ground state with the respective colour scale to the right. We measure the Q function at 441 different analysis displacements α. The π pulse on the qubit $X_\pi^{n=0}$ is conditioned on having no photons in the cavity after the analysis displacement. **c**, Linecut of Q_0 of the ground state along $\mathrm{Im}(\alpha)=0$. The red line is a plot of the theory, a Gaussian given by $\frac{1}{\pi}\mathrm{e}^{-|\alpha|^2}$. A fit to the data with a Gauss function $\frac{1}{\pi}\mathrm{e}^{-I^2/2\sigma^2}$ results in $2\sigma^2=1.03\pm0.02$, which is consistent with the expected width. **d**, Density plot of Q_1 of the ground state with the respective colour scale to the right. In this case the π pulse on the qubit $X_\pi^{n=1}$ is conditioned on having one photon in the cavity after the analysis displacement. **e**, Linecut of Q_1 of the ground state along $\mathrm{Im}(\alpha)=0$. The red line is a plot of the theory given by a Poisson distribution $\frac{1}{\pi}|\alpha|^2\mathrm{e}^{-|\alpha|^2}$.

happens at 385 ns. Figure 3b shows that a Kerr medium can be used as a resource to generate squeezed states[26]. The state is squeezed along the $\mathrm{Re}(\alpha)$ quadrature with a width of 0.88(1), as predicted from theory. The maximum squeezing occurs at $t=58$ ns with a width of Q_0 of 0.87.

After the complete phase collapse, structure re-emerges in the form of multi-component superpositions of coherent states (Fig. 3d–f) at times which are integer submultiples of the complete revival $T_{\mathrm{rev}}=\frac{2\pi}{K}$, Fig. 3h. The revivals, periodically appearing every T_{rev}, can be understood by noting that $\mathrm{e}^{i\frac{K}{2}n^2t}=(-1)^{n^2}$ for $t=T_{\mathrm{rev}}$. The cavity state is then given by $|\Psi(T_{\mathrm{rev}})\rangle=|-\beta\rangle$. At this time, we get a complete state revival to a coherent state with opposite phase. For $t=T_{\mathrm{rev}}/q$, with q an integer larger than 1, we can write the state of the oscillator as a superposition of q coherent states[2]:

$$\left|\Psi\left(\frac{T_{\mathrm{rev}}}{q}\right)\right\rangle=\frac{1}{2q}\sum_{p=0}^{2q-1}\sum_{k=0}^{2q-1}\mathrm{e}^{ik(k-p)\frac{\pi}{q}}\left|\beta\,\mathrm{e}^{ip\frac{\pi}{q}}\right\rangle \quad (3)$$

For $q=2$, we get the two-component Schrödinger cat state, similar to the cat states created in refs 22 and 27. To distinguish the q components of a cat state, the coherent states have to be separated by more than twice their width on a circle with a radius given by the initial displacement. In other words, the coherent states have to be quasi-orthogonal. This means that for a displacement of $|\beta|=2$, the maximum number of coherent states that can be distinguished is 4.

In Fig. 3g, we can see how the state again completely dephases shortly before the coherent revival in Fig. 3h after $t=3{,}065$ ns. After this time, we get a state with amplitude $|\beta|=1.78(2)$, which fits to the expected decay of the resonator state. The theoretical plots for Fig. 3 were simulated by solving a master equation using the decay rate $\kappa/2\pi=10$ kHz of the resonator and introducing a small detuning of 5 kHz of our drive from the resonator frequency ω_c. The time evolution of the state in the experiment agrees well with the theory. The hazy ring that can be seen in theory and experiment in Fig. 3h is produced by cavity decay. The evolution of the state from 0 to 6.05 μs over 50 frames, including two revivals, can be seen in the Supplementary Video.

To get a more quantitative comparison of experiment and theory, we need to determine the quantum state of the resonator. Although in principle one can reconstruct the cavity wavefunction from the measured Husimi Q function, in practice there is important information, such as the interference fringes between coherent state superpositions, which is exponentially suppressed as the separation of the coherent states increases[2]. This makes it hard to distinguish a mixture of coherent states from a coherent superposition in an experiment due to a finite signal to noise ratio. An experimentally more practical way to determine the quantum state of a resonator is, for example, to reconstruct its Wigner function, as this emphasizes the interference fringes. The Wigner function of a cavity[2] has been determined by measuring the parity of the resonator state. More recently, the state of an itinerant microwave field has been determined by measuring the statistical moments of the field operator[28]. Here we use a modified technique, based on earlier work with ion traps and microwave circuits[3,29], to determine the density matrix of the resonator. The main difference is our ability to directly measure $Q_n(\alpha)$, which allows for a simple and efficient measurement and reconstruction of the density matrix of the resonator by using a least square fit to each Q_n (see Supplementary Information). Using this density matrix, we then calculate and plot the Wigner function to show the interference fringes, highlighting the quantum features of the resonator state.

In Fig. 4 we compare the experimentally obtained Wigner functions to a simulation at three different times during the state evolution. The times ($t=2\pi/2K$, $2\pi/3K$ and $2\pi/4K$) were selected such that the Wigner functions correspond to two-, three- and four-component cat states. The simulation was again done by solving a master equation that includes the decay of the cavity. The fidelity $F=\langle\Psi_{\mathrm{id}}|\rho_{\mathrm{m}}|\Psi_{\mathrm{id}}\rangle$ of

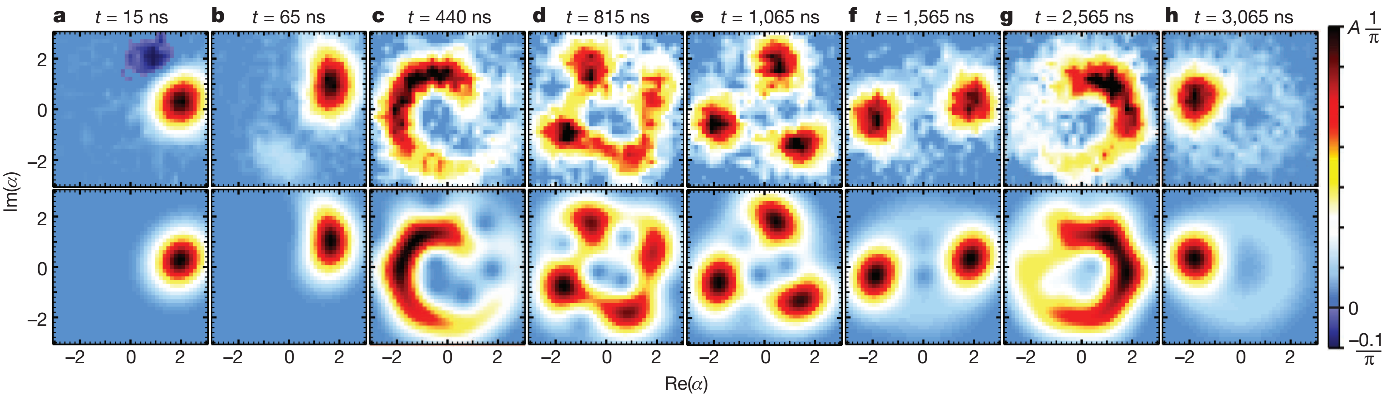

Figure 3 | Time evolution of Q_0 for a coherent state in the nonlinear cavity. Shown are experiment (upper row) and theory (lower row) for a coherent state $\beta = 2$; the time t for the frames shown in **a**–**h** is given above each panel. We measure Q_0 at 441 different analysis displacements α. The resolution of the pictures was doubled by interpolation. Initially the phase of the state spreads rapidly, **a**–**c**, leading to a complete phase collapse after a characteristic time $T_{\mathrm{col}} = \frac{\pi}{2\sqrt{\bar{n}}K} = 385$ ns. For short times, the Kerr interaction leads to a quadrature squeezed state along the Re(α) axis, which can be seen in **b**. After the complete phase collapse, structure emerges again, **d**–**h**, at times which are integer submultiples of the complete revival time $T_{\mathrm{rev}} = \frac{2\pi}{K}$. At these times, one obtains coherent state superpositions which are multi-component cat states, up to a maximum number of resolvable components set by the average photon number in the initial coherent state displacement. The colour scale for Q_0 of each pair of plots is individually rescaled, with the scaling parameter given for **a**–**h** respectively by $A = 1, 0.93, 0.32, 0.24, 0.3, 0.46, 0.24, 0.89$. The negative amplitudes in plot **a** are due to a 10% excited state population of the qubit which evolves in a different rotating frame (see Supplementary Information). This excited state population is not visible in the other frames as it disperses quickly and vanishes in the large positive amplitudes.

the measured state ρ_{m}, compared to an ideal n-component cat state $|\Psi_{\mathrm{id}}\rangle$, consisting of coherent states with amplitude $|\beta| = 2e^{-\kappa t/2}$, is $F_2 = 0.71$, $F_3 = 0.70$, $F_4 = 0.71$ for the two-, three-, four-component cat states, respectively. The Wigner functions show clear interference fringes, which demonstrates that the evolution is indeed coherent and well described by the wavefunction given in equation (2). The main reduction in the fidelity is due to the spurious excited state population of the qubit (see Supplementary Information) and the decay of the resonator state. The decay of the resonator state is also responsible for the asymmetry in the interference fringes of the Wigner function—for example, the maximum of the interference fringes for the two-component cat states is shifted to the left in both theory and experiment.

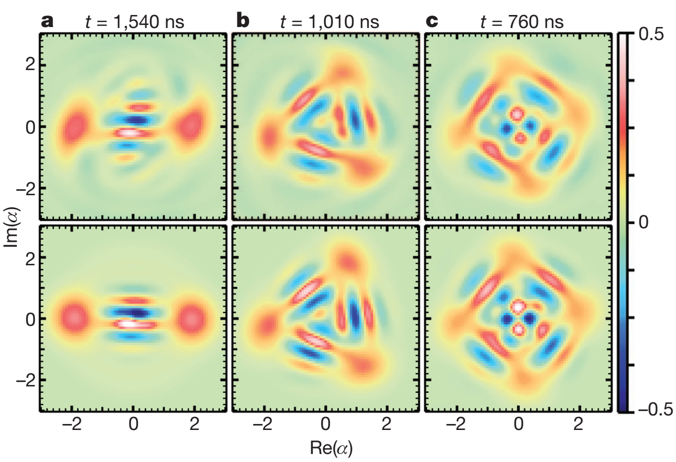

Figure 4 | Wigner function of the multi-component cat states emerging during the Kerr interaction. The top row shows the Wigner functions, reconstructed by cavity state tomography, of a coherent state subject to a Kerr interaction for a time t. The lower row shows the theoretically expected Wigner functions for the same interaction time obtained by a simulation including the decay of the cavity. The Wigner functions are reconstructed from measurements of the quasi probability distributions $Q_n(\alpha)$ for $n = 0$–7. Each $Q_n(\alpha)$ was measured at the same displacements as the corresponding data in Fig. 3. Comparing the experimentally obtained state to an ideal cat state, we find a fidelity $F_2 = 0.71$, $F_3 = 0.70$, $F_4 = 0.71$ for the two-, three- and four-component cats respectively. The experimental data show excellent correspondence with theoretical predictions, including the interference fringes and regions of negative quasi-probability distribution, confirming that highly non-classical states are produced by the Kerr evolution.

We have shown that we can engineer strong photon–photon interactions in a cavity, entering the single-photon Kerr regime where $K \gg \kappa$. We are able to observe the collapse and revival of a coherent state due to the intensity-dependent dispersion between Fock states in the cavity. This opens the possibility of using such a Kerr medium for error correction schemes where a nonlinear cavity is used to realize the necessary components[9]. The good agreement between the theory and the experiment demonstrates the accurate understanding of this system. It also confirms our ability to predict higher-order couplings, which is a necessary ingredient for understanding the behaviour of large circuit QED systems. Furthermore, we have measured the evolution of a coherent state in a Kerr medium at the single-photon level, and shown a new experimental way for creating and measuring multi-component Schrödinger cat states. This demonstrates the ability to create, manipulate and visualize coherent states in a larger Hilbert space, and opens up new directions for continuous variable quantum computation[30].

Received 17 October 2012; accepted 11 January 2013.

1. Wallraff, A. *et al.* Strong coupling of a single photon to a superconducting qubit using circuit quantum electrodynamics. *Nature* **431,** 162–167 (2004).
2. Haroche, S. & Raimond, J. M. *Exploring the Quantum: Atoms, Cavities, And Photons* (Oxford Univ. Press, 2006).
3. Hofheinz, M. *et al.* Synthesizing arbitrary quantum states in a superconducting resonator. *Nature* **459,** 546–549 (2009).
4. Paik, H. *et al.* Observation of high coherence in Josephson junction qubits measured in a three-dimensional circuit QED architecture. *Phys. Rev. Lett.* **107,** 240501 (2011).
5. Yurke, B. & Stoler, D. The dynamic generation of Schrodinger cats and their detection. *Physica B+C* **151,** 298–301 (1988).
6. Braunstein, S. L. Quantum information with continuous variables. *Rev. Mod. Phys.* **77,** 513–577 (2005).
7. Grangier, P., Levenson, J. & Poizat, J. Quantum non-demolition measurements in optics. *Nature* **396,** 537–542 (1998).
8. Peyronel, T. *et al.* Quantum nonlinear optics with single photons enabled by strongly interacting atoms. *Nature* **488,** 57–60 (2012).
9. Kerckhoff, J., Nurdin, H., Pavlichin, D. S. & Mabuchi, H. Designing quantum memories with embedded control: photonic circuits for autonomous quantum error correction. *Phys. Rev. Lett.* **105,** 040502 (2010).
10. Milburn, G. Quantum optical Fredkin gate. *Phys. Rev. Lett.* **62,** 2124–2127 (1989).
11. Saleh, B. E. A. & Teich, M. C. *Fundamentals of Photonics* (Wiley Series in Pure and Applied Optics, 1991).

12. Slusher, R. E., Hollberg, L., Yurke, B., Mertz, J. & Valley, J. Observation of squeezed states generated by four-wave mixing in an optical cavity. *Phys. Rev. Lett.* **55,** 2409–2412 (1985).
13. Franken, P., Hill, A., Peters, C. & Weinreich, G. Generation of optical harmonics. *Phys. Rev. Lett.* **7,** 118–119 (1961).
14. Fisher, R. A., Kelley, P. L. & Gustafson, T. K. Subpicosecond pulse generation using the optical Kerr effect. *Appl. Phys. Lett.* **14,** 140–143 (1969).
15. Nigg, S. E. *et al.* Black-box superconducting circuit quantization. *Phys. Rev. Lett.* **108,** 240502 (2012).
16. Bourassa, J., Beaudoin, F., Gambetta, J. M. & Blais, A. Josephson-junction-embedded transmissionline resonators: from Kerr medium to in-line transmon. *Phys. Rev. A* **86,** 013814 (2012).
17. Bergeal, N. *et al.* Phase-preserving amplification near the quantum limit with a Josephson ring modulator. *Nature* **465,** 64–68 (2010).
18. Yurke, B. *et al.* Observation of 4.2-K equilibrium-noise squeezing via a Josephson-parametric amplifier. *Phys. Rev. Lett.* **60,** 764–767 (1988).
19. Yin, Y. *et al.* Dynamic quantum Kerr effect in circuit quantum electrodynamics. *Phys. Rev. A* **85,** 023826 (2012).
20. Hoffman, A. *et al.* Dispersive photon blockade in a superconducting circuit. *Phys. Rev. Lett.* **107,** 053602 (2011).
21. Shalibo, Y. *et al.* Direct Wigner tomography of a superconducting anharmonic oscillator. Preprint at http://arXiv.org/abs/1208.2441 (2012).
22. Meekhof, D. M., Monroe, C., King, B. E., Itano, W. M. & Wineland, D. J. Generation of nonclassical motional states of a trapped atom. *Phys. Rev. Lett.* **76,** 1796–1799 (1996).
23. Greiner, M., Mandel, O., Hänsch, T. W. & Bloch, I. Collapse and revival of the matter wave field of a Bose-Einstein condensate. *Nature* **419,** 51–54 (2002).
24. Johnson, B. R. *et al.* Quantum non-demolition detection of single microwave photons in a circuit. *Nature Phys.* **6,** 663–667 (2010).
25. Solano, E. Selective interactions in trapped ions: state reconstruction and quantum logic. *Phys. Rev. A* **71,** 013813 (2005).
26. Milburn, G. Quantum and classical Liouville dynamics of the anharmonic-oscillator. *Phys. Rev. A* **33,** 674–685 (1986).
27. Deléglise, S. *et al.* Reconstruction of non-classical cavity field states with snapshots of their decoherence. *Nature* **455,** 510–514 (2008).
28. Eichler, C., Bozyigit, D. & Wallraff, A. Characterizing quantum microwave radiation and its entanglement with superconducting qubits using linear detectors. *Phys. Rev. A* **86,** 032106 (2012).
29. Leibfried, D. *et al.* Experimental determination of the motional quantum state of a trapped atom. *Phys. Rev. Lett.* **77,** 4281–4285 (1996).
30. Leghtas, Z. *et al.* Hardware-efficient autonomous quantum error correction. Preprint at http://arXiv.org/abs/1207.0679 (2012).

Supplementary Information is available in the online version of the paper.

Acknowledgements We thank M. H. Devoret, M. D. Reed, M. Hatridge and A. Sears for discussions. This research was supported by the National Science Foundation (NSF) (PHY-0969725), the Office of the Director of National Intelligence (ODNI), Intelligence Advanced Research Projects Activity (IARPA) through the Army Research Office (W911NF-09-1-0369), and the US Army Research Office (W911NF-09-1-0514). Use of facilities was supported by the Yale Institute for Nanoscience and Quantum Engineering (YINQE) and the NSF (MRSECDMR 1119826). S.M.G. acknowledges support from the NSF (DMR-1004406). M.M. and Z.L. acknowledge support from French Agence Nationale de la Recherche under the project EPOQ2 (ANR-09-JCJC-0070). S.E.N. acknowledges support from the Swiss NSF. E.G. acknowledges support from EPSRC (EP/I026231/1).

Author Contributions G.K. and B.V. performed the experiments. G.K., B.V., Z.L. and M.M. analysed the data. G.K., B.V. and L.F. fabricated the qubits. G.K., B.V., H.P. and S.E.N. designed the device and calculated the device parameters. G.K., E.G., S.M.G. and R.J.S. conceived the experiment and all authors co-wrote the paper.

Author Information Reprints and permissions information is available at www.nature.com/reprints. The authors declare no competing financial interests. Readers are welcome to comment on the online version of the paper. Correspondence and requests for materials should be addressed to R.J.S. (robert.schoelkopf@yale.edu).